A Robust Camera Self-calibration Method Based on Circular Oblique Images

Zhiying Li [1, †], Sitong Li [1, 2, †], Wei Qin [1], Pengjie Tao [1, 3, *]

[1] School of Remote Sensing and Information Engineering, Wuhan University, Wuhan 430079, China
[2] Delft University of Technology, 2628 BL, Delft, The Netherlands
[3] Hubei Luojia Laboratory, Wuhan 430079, China

Keywords: Camera self-calibration, Bundle adjustment, Circular oblique images, Correlation between intrinsic and extrinsic elements.

Abstract

It is crucial to calibrate the camera’s intrinsic orientation elements and distortion parameters to ensure the photogrammetric accuracies. However, using nadir images to perform this task often leads to correlation between the intrinsic and extrinsic orientation elements, which will result in different camera calibration results by using different self-calibration strategies. It even has an impact on the follow-up processes and makes the product accuracy declined. To overcome this challenge, a robust camera calibration method based on circular oblique images was developed in this study. Firstly, circular oblique images with different viewing angles and camera distances were captured by unmanned aerial vehicle, following a specially designed circular flight path. Then the camera parameters were solved through the self-calibration bundle adjustment based on the circular oblique images. The experiments were carried out to compare the robustness and accuracy of nadir-image-based and circular-oblique-image-based methods. The standard deviation of focal lengths solved by different self-calibration strategies reduced from 12.99 pixels to 1.72 pixels, proving that the proposed method weakens the correlation between the intrinsic and extrinsic orientation elements and has strong robustness. The accuracy of aerial triangulation based on the camera parameters solved by the proposed method improved from 34.7 cm to 3.5cm, illustrating the effectiveness of the proposed method.

1. Introduction

Nowadays, unmanned aerial vehicle (UAV) images are widely used in photogrammetry tasks and applications (Roncella et al.,2021; Peppa et al., 2019). However, UAVs often carry consumer-grade, non-metric cameras, which usually have obvious lens distortion (Elhalawani et al., 2021; Simarro et al., 2021). Therefore, camera calibration needs to be performed. Camera calibration refers to calibrating the intrinsic orientation elements and distortion parameters produced during the camera manufacturing process and flight process (Huang et al., 2021). Errors in camera parameters, including focal length, principal point offset, and distortion parameters, will be passed to subsequent steps, affecting the aerial triangulation, making it difficult to restore the relative geometric relationship between the camera center and the image (Zhang et al., 2009).

Camera calibration methods can be categorized into field calibration (Wiącek, 2020; Hou et al., 2020) and self-calibration (Udin et al., 2011; Zheng et al., 2012). Field calibration is known for its high accuracy and is often employed for precision camera calibration, as highlighted by Cao et al. (2015). However, non-metric cameras typically exhibit variable geometric distortion parameters that can change with each flight, necessitating frequent calibration. Therefore, to reduce costs, the self-calibration method is commonly preferred. This method establishes a detailed physical imaging and projection model (Fetzer et al., 2021). It incorporates additional parameters like lens distortion into the collinearity equation to form an error model and only requires a few images to recover all the intrinsic and extrinsic orientation elements of the camera without considering the photographic reconstruction process of the image sequence (Triggs et al., 2000). As a result, self-calibration has gained widespread adoption in the community of photogrammetry and computer vision and mainstream three-dimensional reconstruction software has utilized different self-calibration strategies.

However, there are still certain problems in the self-calibration methods. During conventional UAV photography, the camera is always pointed vertically toward the ground to obtain nadir images. Since the height, angle and direction of the camera remain unchanged during the photography process, there is strong correlation between the intrinsic and extrinsic orientation elements (Duran et al., 2021; Yang et al., 2014). The correlation will result in large differences in the camera self-calibration results for the same set of images when selecting different initial values and using different self-calibration strategies. In addition, when processing a large quantity of images, the method struggles to align all the images uniformly with the infinity plane of the photographic space, leading to unstable calibration results (Chuang et al., 2021). Moreover, the process of aerial triangulation requires linearization, which results in too much computational effort to solve the equation. A more accurate self-calibration initial value needs to be solved in the early stage to ensure convergence.

Therefore, further research is needed on how to obtain stable camera calibration solutions and provide accurate initial values for the subsequent aerial triangulation. This study proposes a robust camera self-calibration method based on circular oblique images, which weakens the correlation between the intrinsic and extrinsic orientation elements through changing the way of photography. Before or after the conventional photography task of nadir images, a local area is selected as the calibration field. Surround the calibration field, a circular flight path is specially designed. Then, following the path, several oblique images with different viewing angles and camera distances are captured by UAV. Finally, camera parameters are solved by performing self-calibration bundle adjustment on the circular oblique images. The experiments show the robustness of camera calibration solutions and the effectiveness of the parameters as the initial values of aerial triangulation.

* Corresponding author
† Contributed equally to this work

2. Methodology

2.1 Self-calibration bundle adjustment

Camera calibration includes calibration of intrinsic orientation elements (focal length f, image principal point coordinates (x_0, y_0)) and lens distortion parameters (Brown, 2002; Cui et al., 2018). The lens distortion of the camera includes radial distortion and tangential distortion (Fraser, 1998). Radial distortion is the deviation of the image point from its actual position in the radial direction. Tangential distortion causes the position of the image point to change both along the radial direction and perpendicular to the radial direction. Its function model is as follows.

$$\begin{cases} \Delta x = (x - x_0)(k_1 r^2 + k_2 r^4 + k_3 r^6) + p_1(r^2 + 2(x - x_0)^2) + 2p_2(x - x_0)(y - y_0) \\ \Delta y = (y - y_0)(k_1 r^2 + k_2 r^4 + k_3 r^6) + p_2(r^2 + 2(y - y_0)^2) + 2p_1(x - x_0)(y - y_0) \end{cases} \quad (1)$$

Where (x, y) is the image point coordinates; $(\Delta x, \Delta y)$ is the deformation of image point coordinates; r is the radiation distance of the image point; k_1, k_2, k_3 are radial distortion parameters; p_1, p_2 are tangential distortion parameters.

The self-calibration bundle adjustment establishes a rigorous physical model, which makes it easier to use additional parameters as observation values and participate in the construction of error equations to achieve offset compensation of various system errors (Shan, 2018).

Assume that the coordinates of the camera center in the object space coordinate system are (X_S, Y_S, Z_S), the coordinates of any ground point P are (X, Y, Z), the image coordinates of the image point p corresponding to point P on the image are $(x, y, -f)$. According to the collinearity equation and considering the influence of lens distortion $\Delta x, \Delta y$, the camera imaging model is obtained as shown in Equation (2).

$$\begin{cases} x - x_0 + \Delta x = -f \frac{a_1(X - X_S) + b_1(Y - Y_S) + c_1(Z - Z_S)}{a_3(X - X_S) + b_3(Y - Y_S) + c_3(Z - Z_S)} \\ y - y_0 + \Delta y = -f \frac{a_2(X - X_S) + b_2(Y - Y_S) + c_2(Z - Z_S)}{a_3(X - X_S) + b_3(Y - Y_S) + c_3(Z - Z_S)} \end{cases} \quad (2)$$

where $a_{ij} (1 \le i, j \le 3)$ are elements of the rotation matrix R, related to the extrinsic orientation elements φ, ω, κ, as shown in Equation (3) and Equation (4).

$$R = \begin{bmatrix} a_1 & a_2 & a_3 \\ b_1 & b_2 & b_3 \\ c_1 & c_2 & c_3 \end{bmatrix} \quad (3)$$

$$\begin{cases} a_1 = cos\varphi cos\kappa - sin\varphi sin\omega sin\kappa \\ a_2 = -cos\varphi sin\kappa - sin\varphi sin\omega cos\kappa \\ a_3 = -sin\varphi cos\omega \\ b_1 = cos\omega sin\kappa \\ b_2 = cos\omega cos\kappa \\ b_3 = -sin\omega \\ c_1 = sin\varphi cos\kappa + cos\varphi sin\omega sin\kappa \\ c_2 = -sin\varphi sin\kappa + cos\varphi sin\omega cos\kappa \\ c_3 = cos\varphi \end{cases} \quad (4)$$

At this time the error equation based on the collinearity equation should be Equation (5).

$$V = AX_1 + BX_2 + CX_3 - L \quad (5)$$

Where V is residual error vector; A, B, C are all the coefficient matrix of the error equation; $X_1 = [\Delta X_S \ \Delta Y_S \ \Delta Z_S \ \Delta\varphi \ \Delta\omega \ \Delta\kappa]^T$ is the correction vector of the extrinsic orientation elements; X_2 is the correction vector of the ground coordinates; X_3 is the correction vector of the self-calibration parameters; L is a constant term.

2.2 Correlation analysis of the intrinsic and extrinsic elements

In traditional self-calibration methods, the nadir images are often used. The photography baseline is a straight line, the flight height remains approximately unchanged, and the principal optical axis is almost parallel and approximately perpendicular to the photography baseline.

Since the flight height keeps approximately unchanged during the photography process, there is a strong correlation between the focal length of the nadir image and the camera distance, as shown in Figure 1; the principal optical axis is approximately perpendicular to the baseline, resulting in a strong correlation between the principal point coordinates of the image and the extrinsic orientation elements X_S, Y_S. This correlation between the intrinsic and extrinsic orientation elements will lead to unstable self-calibration results. The camera parameters obtained by different solution methods are often different.

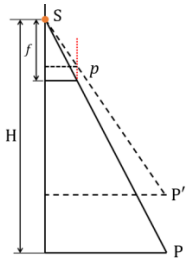

Figure 1. Correlation between the focal length f and camera distance H

Under ideal vertical photography conditions, the pitch angle φ, roll angle ω are both approximately zero, while the yaw angle κ within the same route are similar. Under this condition, let $\varphi = \omega = 0$, remain κ unchanged. The elements of coefficient matrix A can be shown as Equation (6)

$$\begin{cases} a_{11} = \frac{\partial x}{\partial X_s} = -\frac{f}{H} cos\kappa \\ a_{12} = \frac{\partial x}{\partial Y_s} = -\frac{f}{H} sin\kappa \\ a_{13} = \frac{\partial x}{\partial Z_s} = -\frac{x}{H} \\ a_{14} = \frac{\partial x}{\partial \varphi} = -\left(f + \frac{x^2}{f}\right) cos\kappa + \frac{xy}{f} sin\kappa \\ a_{15} = \frac{\partial x}{\partial \omega} = -\frac{xy}{f} cos\kappa - \left(f + \frac{x^2}{f}\right) sin\kappa \\ a_{16} = \frac{\partial x}{\partial \kappa} = y \\ a_{21} = \frac{\partial y}{\partial X_s} = -\frac{f}{H} sin\kappa \\ a_{22} = \frac{\partial y}{\partial Y_s} = -\frac{f}{H} cos\kappa \\ a_{23} = \frac{\partial y}{\partial Z_s} = -\frac{y}{H} \\ a_{24} = \frac{\partial y}{\partial \varphi} = -\frac{xy}{f} cos\kappa + \left(f + \frac{y^2}{f}\right) sin\kappa \\ a_{25} = \frac{\partial y}{\partial \omega} = -\left(f + \frac{y^2}{f}\right) cos\kappa - \frac{xy}{f} sin\kappa \\ a_{26} = \frac{\partial y}{\partial \kappa} = -x \end{cases} \quad (6)$$

Comparing the coefficient values, it can be seen that since the height, angle and direction of the nadir images are always consistent, the coefficient of the camera center translation parameter ($\begin{bmatrix} a_{11} & a_{12} & a_{13} \\ a_{21} & a_{22} & a_{23} \end{bmatrix}$) has a linear correlation with the intrinsic orientation elements. It will produce a normal equation that is close to singular, causing the solution of the normal equation to be unstable. Different solution methods may obtain different intrinsic orientation elements and distortion parameters.

2.3 Correlation elimination method based on circular oblique images

The main reason why the self-calibration bundle adjustment of nadir images cannot obtain a stable solution is the strong correlation between the intrinsic and extrinsic orientation elements. And the correlation is generated by the camera's height, angle and direction being constant throughout the flight. Therefore, by planning new routes and flight patterns, correlations can be artificially weakened. This study proposes a method that performs self-calibration bundle adjustment based on the circular oblique images to weaken the correlation and obtain a stable solution, whose calibration parameters will be used for the processing of nadir images of the target area.

A circular flight path is designed to obtain circular oblique images, as shown in Figure 2. The UAV flies in a rotating circle at different altitudes around a target in a local area. During the photography process, the angle of the principal optical axis is fixed. For the planning of the flight path, the target radius of the circular flight $R \approx tan\theta$ is estimated from the photographic height H and tilt angle θ. The tilt angle θ is generally 30°.

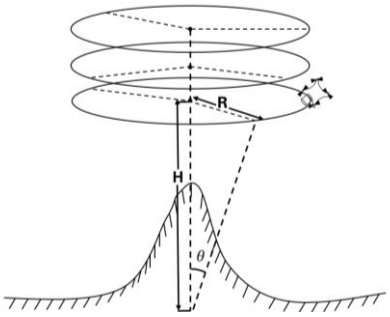

Figure 2. The circular flight paths

During circular photography, the UAV obtains several circular oblique images of a certain area, by adjusting the flight height, camera position and the angle between the principal optical axis and the ground. Since when circling and flying, the camera height and direction of the image in the dataset change greatly, but the camera parameters always remain unchanged, so when performing self-calibration bundle adjustment on the circular oblique images, the correlation between the intrinsic and extrinsic orientation elements is weakened, resulting in stable camera parameters. Specifically, capturing images at different heights can effectively overcome the correlation between the camera distance and the focal length; at the moment of capturing, the principal optical axis is at a certain angle with the ground and flies around, which can effectively overcome the correlation between the principal point and the extrinsic orientation line elements.

In addition, since the principal optical axis of the circular flight has a certain inclination angle and always points to the same target, there is high overlap and strong constraints among images, which is conducive to further improving the accuracy of calibration.

3. Experiments and results

To weaken the correlation between the intrinsic and extrinsic orientation elements and obtain a stable camera parameter solution, this section tests the proposed camera self-calibration method based on the circular oblique images. Different software is used to conduct camera parameter stability comparison and test the usability of the self-calibration parameters solved from the circular oblique images.

3.1 Test area and circular flight planning

The test area consists of calibration area and validation area. In the validation area, nadir images and ground points are obtained to test the usability and accuracy of the proposed method. The calibration area is a local area selected for circular flight to obtain the circular oblique images.

In the experiments, the validation area is located in the campus of Wuhan University. The overall terrain is flat, with a slightly higher altitude from south to north. It contains buildings, vegetation, lakes and other features. A square with a statue was selected as the calibration area, and a circular flight was designed to obtain circular oblique images. When selecting calibration area, due to the special flight trajectory, it is necessary to avoid collisions between the flying platform and surrounding features. The Footprints of camera stations and overview of the calibration area and validation area are shown in the Figure 3.

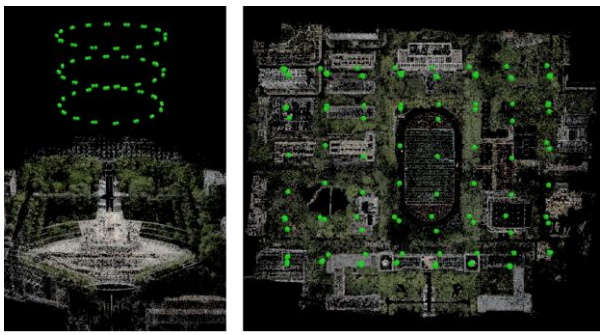

Figure 3. Footprints of camera stations and overview of the calibration area and validation area

The DJI M300 UAV was selected as flying platform which carried a Zenmuse P1 full-frame camera with a focal length of 35 *mm* to obtain nadir images and circular oblique images. The image size is 8192×5460 *pixels*, and the pixel size is 4.4 μm.

The UAV flew around the calibration area for 3 circles at altitudes of 80 meters, 100 meters, and 120 meters and obtained a total of 100 images. The principal optical axis will always maintain a certain angle with the ground. Then it captured 120 nadir images in the validation area.

In the data processing stage, different self-calibration strategies were used to prove the existence of correlation between the intrinsic and extrinsic orientation elements. Agisoft Metashape, ContextCapture and Pix4Dmapper, which are widely used in the photogrammetry and UAV surveying and mapping, were selected to perform the aerial triangulation to solve intrinsic orientation elements and distortion parameters of the camera.

The experiments were conducted with and without GPS. In the validation area, ten ground points were obtained as check points to assess the accuracy, and four of them were selected as control points when GPS was not used. The distribution of the ground points was as shown in Figure 4.

Figure 4. Distribution of ground control points (marked as red triangles) and check points

3.2 Correlation test of the intrinsic and extrinsic orientation elements

3.2.1 Test settings

To verify the correlation between the intrinsic and extrinsic orientation elements of the nadir images, and the impact of the correlation on the solution of the intrinsic orientation elements and distortion parameters, different photogrammetry software was used to perform aerial triangulation with and without GPS. The results were compared and discussed about the correlation.

In addition, under general conditions, several photos were selected to solve the correlation coefficient matrix between the intrinsic and extrinsic orientation elements, which can further prove the existence of correlation.

3.2.2 Camera parameter results of different software under different conditions

The results solved by different software are shown in Table 1.

Images	Software	GPS	f	x_0	y_0	k_1	k_2	k_3	p_1	p_2
Nadir images	ContextCapture	√	8183.57	4099.63	2769.16	-0.0490	0.0172	-0.0918	-0.00155	0.00224
		×	8184.09	4099.61	2769.20	-0.0489	0.0172	-0.0917	-0.00155	0.00224
	Agisoft Metashape	√	8197.50	4100.08	2769.57	-0.0486	0.0182	-0.0960	-0.00156	0.00224
		×	8194.60	4100.23	2769.58	-0.0496	0.0202	-0.1004	-0.00154	0.00223
	Pix4Dmapper	√	8209.52	4099.45	2770.37	-0.0506	0.0214	-0.0996	-0.00156	0.00224
		×	8102.58	4097.96	2766.50	-0.0505	0.0177	-0.0869	-0.00149	0.00214
Circular oblique images	ContextCapture	√	8199.08	4100.83	2766.42	-0.0512	0.0264	-0.1084	-0.00163	0.00221
		×	8199.01	4100.79	2766.56	-0.0512	0.0263	-0.1082	-0.00163	0.00221
	Agisoft Metashape	√	8200.64	4101.63	2765.75	-0.0507	0.0238	-0.1051	-0.00163	0.00223
		×	8200.09	4101.56	2765.79	-0.0507	0.0233	-0.1043	-0.00164	0.00222
	Pix4Dmapper	√	8197.21	4098.86	2765.95	-0.0511	0.0268	-0.1090	-0.00169	0.00212
		×	8189.10	4099.10	2769.74	-0.0511	0.0275	-0.1091	-0.00160	0.00209

Table 1. Self-calibration results of different software under different conditions (uint: pixels)

Table 2 shows the standard deviations of the intrinsic orientation elements solved under different conditions.

Images	GPS	σ_f	σ_{x0}	σ_{y0}
Nadir images	√	12.99	0.33	0.61
	×	50.37	1.17	1.68
Circular oblique images	√	1.72	1.43	0.34
	×	6.06	1.26	2.09

Table 2. Standard deviations of the intrinsic orientation elements solved under different conditions (unit: pixels)

The intrinsic orientation elements and distortion parameters solved by different software with different self-calibration strategies based on nadir images vary greatly. Taking the focal length f as an example, the results from ContextCapture, Agisoft Metashape and Pix4Dmapper are respectively 8184.09, 8194.60 and 8102.58 pixels without GPS. The maximum difference is 92.02 pixels, and the standard deviation is 50.37 pixels. When GPS constraints are used, the standard deviation decreases to 12.99 pixels, but is still large. Because of the correlation between the intrinsic and extrinsic orientation elements, the self-calibration parameters based on difference self-calibration strategies vary a lot.

When self-calibration is performed based on circular oblique images, the results become much more stable. With the constraint of GPS, the standard deviations of the focal length f and image principal point coordinates (x_0, y_0) are 1.72, 1.43, 0.34 pixels, respectively. And without GPS, they are 6.06,1.26, 2.09 pixels, respectively. Under different conditions, the paraments solved by different software remain within a stable range, with small differences. It demonstrates that the self-calibration parameters solved based on circular oblique images are more stable and the proposed method has strong robustness.

In conclusion, the self-calibration method based on circular oblique images is much more robust than that based on nadir images. It has better performance on weakening the correlation between the intrinsic and extrinsic orientation elements.

3.2.2 Correlation coefficient matrix of the intrinsic and extrinsic orientation elements

Several photos were selected to solve the correlation coefficient matrix, and the result is shown in Table 3. The correlation coefficient between the focal length f and camera distance Z reached 0.783, which means that there is a high correlation between f and Z. In addition, there are also positive correlations between the image principal point coordinates y_0 and camera distance Z whose correlation coefficient is 0.210, between the image principal point coordinates x_0 and roll angle ω whose correlation coefficient is 0.136. These data further prove the

existence of correlation between the intrinsic and extrinsic orientation elements.

	X	*Y*	*Z*	*φ*	*ω*	*κ*
f	-0.003	-0.024	**0.783**	-0.018	0.028	-0.014
x_0	-0.019	-0.005	0.010	-0.022	0.136	0.046
y_0	-0.002	-0.035	0.210	0.089	-0.027	-0.039
k_1	-0.148	0.123	-0.162	-0.151	0.133	-0.003
k_2	0.020	0.001	0.044	0.021	0.003	0.002
k_3	-0.024	-0.003	0.005	-0.026	-0.001	-0.003
p_1	-0.010	-0.009	-0.111	0.076	-0.017	-0.047

Table 3. Correlation coefficient matrix of the intrinsic and extrinsic orientation elements solved from nadir images

3.3 Effectiveness of circular oblique image self-calibration parameters

3.3.1 Test settings

To verify the effectiveness of the proposed camera self-calibration method based on circular oblique images, two sets of experiments were designed.

(1) Pre-calibrate camera parameters using circular oblique images. Camera parameters were firstly pre-calibrated by aerial triangulation based on the circular oblique images; then the pre-calibrated camera parameters are used as true values in the aerial triangulation of nadir images; finally, the accuracy is evaluated using ground check points.

(2) Self-calibrate camera parameters using nadir images. Only nadir images were used to perform aerial triangulation, and directly used check points to calculate accuracy.

3.3.2 Accuracy comparison

(1) with GPS information

Table 4 shows the accuracy of the bundle adjustment of nadir images using pre-calibrated camera parameters and self-calibrated camera parameters respectively with GPS.

Points	Errors using pre-calibrated parameters (cm)			Errors using self-calibrated parameters (cm)		
	ΔX	ΔY	ΔZ	ΔX	ΔY	ΔZ
1	-6.3	-5.5	5.7	-0.5	-6.4	39.8
2	-6.3	-8.2	-1.9	-0.7	-10.2	31.4
3	-5.3	-11.1	2.7	0.2	-12.5	36.3
4	-4.5	-7.9	-0.7	0.0	-10.7	36.1
5	-6.5	-7.7	-2.4	-1.2	-10.6	33.9
6	-6.4	-6.8	-1.5	-0.4	-9.9	35.6
7	-5.0	-5.7	0.7	-1.8	-8.6	38.3
8	-0.2	-10.0	-5.2	3.2	-12.0	31.9
9	0.1	-7.5	-5.3	2.7	-8.6	31.2
10	-5.1	-7.1	-4.2	-0.7	-8.0	31.1
RMSE	**5.1**	**7.9**	**3.5**	1.5	9.9	34.7

Table 4. Errors of ground check points after bundle adjustment using pre-calibrated and self-calibrated camera parameters with GPS

When only nadir images were used in the camera calibration, the maximum vertical error of ground check points after aerial triangulation reaches 39.8 cm. The root mean square errors (RMSEs) of X, Y, Z coordinates are 1.5 cm, 9.9 cm, and 34.7 cm, respectively.

When using the proposed self-calibration method based on circular oblique images, the pre-calibrated camera parameters were used as the true values to perform aerial triangulation on the nadir images. In this case, the maximum vertical error of ground check points is reduced from 39.8 cm to 5.7 cm. while the vertical RMSE is reduced from 34.7cm 3.5 cm.

(2) without GPS information

When there is no GPS constraint, four ground points located at the edge of the test area were selected as control points, and other points were used as check points as shown in Figure 4. The accuracy of the bundle adjustment of nadir images using pre-calibrated camera parameters and self-calibrated camera parameters respectively without GPS are obtained as shown in Table 5.

Points	Errors using pre-calibrated parameters (cm)			Errors using self-calibrated parameters (cm)		
	ΔX	ΔY	ΔZ	ΔX	ΔY	ΔZ
1	0.2	0.9	-3.4	18.9	-18.3	-89.7
2	3.0	-0.2	-2.8	36.3	10.6	-125.3
3	4.6	-2.6	-4.6	17.7	2.5	-60.7
4	0.8	-3.4	3.2	3.9	-27.7	-71.6
5	-1.0	-0.9	-0.8	-8.3	-12.6	53.1
6	0.8	-0.3	-0.6	-8.9	-14.1	65.6
RMSE	**2.3**	**1.8**	**2.9**	18.9	16.2	81.3

Table 5. Errors of ground check points after bundle adjustment using pre-calibrated and self-calibrated camera parameters without GPS

When GPS constraint is not available, the bundle adjustment using self-calibrated camera parameters did not achieve ideal results. The RMSEs of X, Y, Z coordinates of the check points are 18.9 cm, 16.2 cm, and 81.3 cm, respectively. Compared to the experiment with GPS, the accuracies drop seriously.

When self-calibration is performed based on circular oblique images, the addition of pre-calibrated camera parameters allows the aerial triangulation results to maintain higher accuracy. The RMSEs of X, Y, Z coordinates are 2.3cm, 1.8cm and 2.9cm respectively, with much improvement compared to the self-calibrated parameters. And since the control points were used when conducting experiments without GPS, the accuracy is higher than the results with GPS.

In conclusion, the pre-calibrated camera parameters can be used for aerial triangulation of nadir images, which can obtain higher-precision results.

4. Conclusion

This study addresses the challenge of weakening the correlation between the intrinsic and extrinsic orientation elements and obtains a stable solution during the camera calibration process. This paper studies a robust camera self-calibration method based on circular oblique images, which adopts a new data acquisition and use strategy to obtain stable camera calibration solutions. Through a combination of theoretical derivation and experiments, the existence of correlations between the position of the image principal point and the extrinsic orientation line elements, and the focal length and the camera distance is proved. In practical aerial photography missions, additional circular flight photography is performed over specific areas or target. During image processing, the self-calibration bundle adjustment is performed on the circular oblique images, and the solved camera parameters are used for the subsequent aerial

triangulation of the nadir images. Compared the self-calibration experiments based on the nadir images and circular oblique images, the standard deviations of focal lengths solved by different self-calibration strategies are reduced from 12.99 pixels to 1.72 pixels, which proves that the proposed method has weakened the correlation between the intrinsic and extrinsic orientation elements. The accuracy of bundle adjustment based on the camera parameters solved by the proposed method improved from 34.7 cm to 3.5 cm, illustrating the effectiveness of the self-calibration method based on circular oblique images.

References

Brown D.C., 2002. Close-Range Camera Calibration. *Photogrammetric Engineering*, 37(8), 855-866.

Cao L.Z., Yang L., Kan P.T., Jia Y., Zhang W.G., 2015. Calibration of non-metric digital camera based on calibration filed. *Science of Surveying and Mapping*, 40(02), 132-137.

Chuang J.H., Ho C.H., Umam A., Chen H.Y., Hwang J.N., Chen T.A., 2021. Geometry-based camera calibration using closed-form solution of principal line. *IEEE Transactions on Image Processing*, 30, 2599-2610.

Cui C.C., Wang J.L., Ma Z.L., 2018. The iterative method of camera calibration. *Bulletin of surveying and mapping*, 6, 50-54.

Duran Z., Atik M., 2021. Accuracy comparison of interior orientation parameters from different photogrammetric software and direct linear transformation method. *International Journal of Engineering*, 6, 74-80.

Elhalawani M.A., Zeidan Z.M., Beshr A.A., 2021. Implementation of close range photogrammetry using modern non-metric digital cameras for architectural documentation. *Geodesy and Cartography*, 47(1), 45-53.

Fetzer T., Reis G., Stricker D., 2020. Stable Intrinsic Auto-Calibration from Fundamental Matrices of Devices with Uncorrelated Camera Parameters. *2020 IEEE Winter Conference on Applications of Computer Vision (WACV)*, 221-230.

Fraser C, 1998. Automated processes in digital photogrammetric calibration. *Orientation, and Triangulation, Digital Signal Processing*, 8(4), 277-283.

Hou Y., Su X., Chen W., 2020. Alignment method of an axis based on camera calibration in a rotating optical measurement system. *Applied Sciences*, 10(19), 6962.

Huang W., Jiang S., Jiang W., 2021. Camera Self-Calibration with GNSS Constrained Bundle Adjustment for Weakly Structured Long Corridor UAV Images. *Remote. Sensing*, 13, 4222.

Omar S.O., 2017. A survey on position-based routing protocols for Flying Ad hoc Networks. *Vehicular Communications*, 10, 29-56.

Peppa M.V., Hall J., Goodyear J., Mills J.P, 2019. Photogrammetric assessment and comparison of DJI Phantom 4 pro and phantom 4 RTK small unmanned aircraft systems. *The International Archives of the Photogrammetry, Remote Sensing and Spatial Information Sciences*, 42, 503-509.

Roncella, R., Forlani, G, 2021. UAV block geometry design and camera calibration: A simulation study. *Sensors*, 21(18), 6090.

Simarro G., Calvete D., Plomaritis T.A., Moreno-Noguer F., Giannoukakou-Leontsini I., Montes J., Durán R., 2021. The influence of camera calibration on nearshore bathymetry estimation from UAV videos. *Remote Sensing*, 13(1), 150.

Triggs B., McLauchlan P.F., Hartley R.I., Fitzgibbon A.W., 2000. Bundle adjustment - a modern synthesis. *International Workshop on Vision Algorithms*, 298-372.

Udin W.S., Ahinad A., 2011. Calibration of high-resolution digital camera using self-calibration bundle adjustment method. *IEEE, International Colloquium on Signal Processing and ITS Applications*, 137-141.

Wiącek P., 2020. The database for multifactorial UAV accuracy assessments. *The International Archives of the Photogrammetry, Remote Sensing and Spatial Information Sciences*, 43, 163-172.

Yang Y.L., Han L., Hu H.Y., 2014. Correction analysis and improvement of Brown self-calibration model. *Bulletin of Surveying and Mapping*, 5, 37-40.

Zhang J.Q., Pan L., 2009. Photogrammetry. *Wuhan: Wuhan University Press*.

Zheng S.Y., Huang R.Y., Guo B.Y., Hu F., 2012. Stereo-camera calibration with restrictive constraints. *Acta Geodaetica et Cartographica Sinica*, 41(06), 877-885.